EARTHQUAKE ENGINEERING AND STRUCTURAL DYNAMICS
Earthquake Engng. Struct. Dyn. **28**, 1637–1649 (1999)

DYNAMICS OF THREE-BLOCK ASSEMBLIES WITH UNILATERAL DEFORMABLE CONTACTS. PART 2: ACTUAL APPLICATION

UGO ANDREAUS* AND PAOLO CASINI

Dipartimento di Ingegneria Strutturale e Geotecnica, Facoltà di Ingegneria, Università degli Studi di Roma 'La Sapienza', Via Eudossiana 18, 00184 Rome, Italy

SUMMARY

On the basis of the formulation of multibody dynamics with deformable contacts presented in Part 1, the dynamic response of the trilith (the simplest scheme of a colonnade belonging to a temple) to half-sine-wave pulse and to horizontal harmonic ground motion is analysed and the influence of bouncing and sliding on the type of motion is studied. Attention has been given to the dependence of the system response on the excitation amplitude and frequency, on the difference of friction between lintel-column and soil-column, and on the block slenderness. As far as half-sine-wave pulse is concerned, rest, stable motion and collapse have been identified; whereas, for harmonic excitation, rest or transient up to failure have been observed: during the transient a wide variety of responses up to chaotic motion has been exhibited. Copyright © 1999 John Wiley & Sons, Ltd.

KEY WORDS: multibody systems; unilateral constraints; impact; friction; dynamics; distinct element method

1. INTRODUCTION

Many works[1–17] have been devoted exclusively to study the motion type and stability of a single block on a moving rigid ground; on the contrary, in spite of the fact that monumental structures are made of many blocks, few papers[18–24] tackled with the dynamic analysis of multi-block structures. Obviously this is due to the fact that dynamics of multibody systems with unilateral constraints do not lead themselves to simple analysis because the absence of connections between elements can give rise to several possible mechanisms. To elaborate further, relevant aspects of the motion can be: rocking, bouncing, slidings with friction, loss of equilibrium due to excessive rotations or relative displacements.[23] For these reasons a general model should be defined, where all the possible degrees of freedom of the system are taken into account.

* Correspondence to: Ugo Andreaus, Dipartimento di Ingegneria Strutturale e Geotecnica, Facoltà di Ingegneria, Università degli Studi di Roma 'La Sapienza', Via Eudossiana 18, Rome 00184, Italy.
E-mail: casini@scilla.ing.uniroma1.it

Contract/grant sponsor: Italian Ministry of University and Scientific Research.

Received 20 October 1998
CCC 0098–8847/99/121637–13$17·50 *Revised 1 April 1999*
 Accepted 6 July 1999

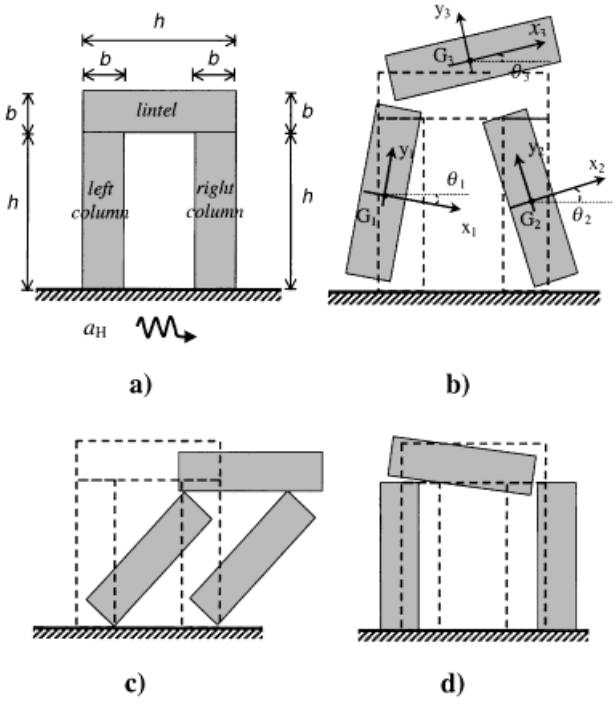

Figure 1. Investigated system. (a) Three-block assembly; (b) degrees-of freedom system; (c) first collapse mode (overall excessive rotation); (d) second collapse mode (coupled effects between excessive slidings and rotations)

The dynamic behaviour of three rigid blocks simply supported on each other has been first investigated by Allen *et al.*[20] They study the motion of such a structure (i.e. a trilith which is the simplest scheme of a colonnade belonging to a temple) excited by half and full cycle displacement pulse, and earthquake components only by means of a single degree-of-freedom model (simple rocking model).

Sinopoli and Sepe[23] study the motion of a trilith, Figure 1(a), excited by horizontal harmonic ground motion and under the assumption that bouncing and the sliding displacements of the two columns with respects to the plane support are negligible: so, in this model, columns exhibit only a rocking motion while sliding between the two columns and the lintel is taken into account. The authors perform a parametric investigation as a function of the excitation parameters and of the mechanical features of the system: they found that collapse by overall excessive rotation, Figure 1(c), is a rather improbable failure mode under seismic loads, whereas collapse due to excessive sliding as a consequence of the coupled dynamics, Figure 1(d), seems to be a probable mode of collapse, which requires a sufficiently long time to occur.

Aim of this paper is to study the dynamics of an assembly made of three rigid blocks simply supported on each other (i.e. connected with unilateral contacts) in the presence of dry friction and excited by a moving foundation, Figure 1(a). Bouncing and sliding displacements between blocks and between columns and ground are allowed here so that all the possible degrees of freedom of the system are considered Figure 1(b). In Part 1, attention has been given to writing

down the analytical formulation of the equations of motion, of the contact kinematics and of the contact laws. Owing to the large number of degrees of freedom and the extreme complexity of the non-smooth dynamical system, an analytical investigation, from a practical point of view, is not advisable; so an analytical–numerical model based on the distinct element method and on the deformable contact formulation, proposed in Part 1, has been used. The dynamic response of the system to half-sine-wave pulse and to horizontal harmonic ground motion will be analysed and influence of bouncing and sliding on the type of motion will be studied. A parametric investigation will be performed as a function of the excitation parameters and of the mechanical features of the system.

2. SYSTEM AND PROCEDURE DESCRIPTION

2.1. Investigated system

We consider the two-dimensional system shown in Figure 1(a), made of three identical rigid blocks of rectangular shape. The height of each block is h and the width is b; θ_i ($i = 1, 2, 3$) are the angles of rotation of the blocks and X_i, Y_i ($i = 1, 2, 3$) are the centroid co-ordinates (Figure 1(b)). The vector $\mathbf{q}^T = \{X_1, Y_1, \theta_1, X_2, Y_2, \theta_2, X_3, Y_3, \theta_3\}$ lists the lagrangian co-ordinates which describes the instantaneous configuration of the system. Each block has mass m and polar moment of inertia about the block centroid I. We assume that $2R = \sqrt{b^2 + h^2}$, $\alpha = \arctan(b/h)$ and $p^2 = 3g/4R$, where g is the gravity acceleration, R and p are, respectively, the half-diagonal and the pseudo-frequency of each block.

The trilithic assembly of Figure 1(a) has been studied where different slenderness values ranging from $\lambda = 4{\cdot}0$ to $12{\cdot}0$ have been considered for each block; moreover, breadth $b = 0{\cdot}12$ m, thickness $0{\cdot}06$ m and mass density 2700 kg/m^3 have been assumed. The numerical response of the system under horizontal half-sine-wave pulse and harmonic excitation applied at ground level has been investigated; the form of the excitation is assumed to be given by

$$a_H = \beta\alpha g \cos(\Omega t) \tag{1}$$

where β is the non-dimensional amplitude, Ω the driving frequency and t the time.

In the figures of the following sections, only rotation degree-of-freedom has been depicted in as much as it has been considered the most representative parameter of the problem under investigation.

2.2. Implementation

We use the deformable contact approach described in Sections 3 and 4 of Part 1. Thus, the equations of motion for each block are given by equations (22) of Part 1 where contact forces obey the contact laws given in Section 4 of Part 1.

The four principal components of the general distinct element simulation system are considered to be: (a) object representation (b) contact detection (c) physics (assembling and solving equations of motion) and (d) visualization. As far as point (b) is concerned we have dealt with the more restricted problem of geometry contact between bodies with specific geometric shape. As far as points (b) and (c) are concerned, the body system is typified by short-range interactions. Moreover, it is characterized by slowly varying topology, that is the objects move only a small

amount and then we can conclude that bodies can make new contacts only with near neighbouring objects; we can then ensure that each object keeps track only of a limited number of objects as potential contactors.

The equations of motion have been numerically solved via an application of the Runge–Kutta–Fehlberg method;[26] an advantage of this method is that one can increase or decrease the step size for the next iteration depending on the value of the estimated error. The numerical results given below have been achieved by assuming a tolerance 5×10^{-5}, which has yielded an integration step range from 1×10^{-4} to 1×10^{-3}.

The parameters of the contact law have been identified by means of the procedure outlined in Reference 25: $U_n = 2 \times 10^{-4}$ m, $k_{ni}^C = 10^4$ kN/m, $k_{ni}^E = k_{ni}^C/3$, $\gamma_c = \gamma_e = 5$, $\bar{\Lambda}_n = \infty$, $\tilde{u}_t = \infty$, $\delta = \infty$, $\varphi_0 = 0$. The different nature of material pairings can require different values of φ_r to be used at the soil–column (φ_s) and lintel–column (φ_l) contacts.

3. NUMERICAL RESULTS

3.1. *Half-sine-wave pulse*

In this case the driving function given by equation (1) holds for $0 \leqslant \Omega t \leqslant \pi$. Three types of motion have been observed: rest, stable motion, and collapse; only one collapse mode was exhibited, i.e. failure by overall excessive rotation, Figure 1(c).

For $\lambda = 4{\cdot}0$ both high ($\varphi_l = 90^\circ$) and low ($\varphi_l = 15^\circ$) friction angles between columns and lintel have been considered and the parametric investigation for $\varphi_s \leqslant \varphi_l$ has led to the survival domain in Figure 2, where three zones can be identified: rest under the dashed line, stable motion between dashed and continuous lines, collapse above the continuous line; it is worth noting that a wider stable zone is exhibited for low friction; ω denotes the non-dimensional frequency Ω/p.

During the stable motion the two columns oscillated in phase and simultaneously exhibited the maximum rotation θ_{MAX}. Figure 3 shows that, for given excitation amplitudes, the maximum rotation decreases as the driving frequency increases; furthermore, for given excitation amplitudes and driving frequency, maximum rotation decreases according to friction. Grey lines refer to $\varphi_s = \varphi_l = 90^\circ$ and black lines to $\varphi_s = \varphi_l = \arctan(\lambda^{-1})$. Finally, maximum rotation increases

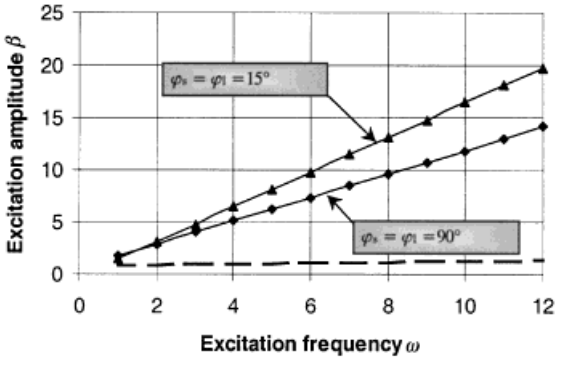

Figure 2. Survival domain (*half sine-wave pulse*)

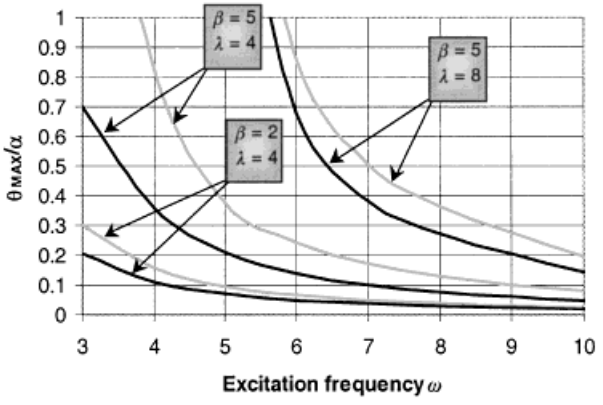

Figure 3. Maximum rotation *versus* excitation frequency for $\varphi_s = \varphi_1 = 90^\circ$ (grey lines) and $\varphi_s = \varphi_1 = \arctan(\lambda^{-1})$ (black lines)

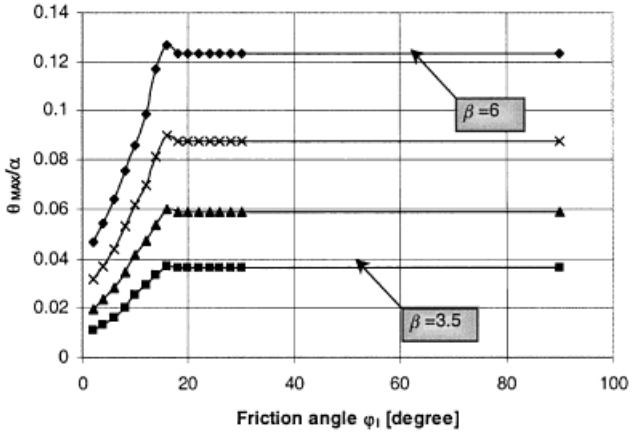

Figure 4. Maximum rotation *versus* friction angle φ_1 for $\varphi_s = 90^\circ$ and $\omega = 10{\cdot}0$

according to slenderness; for the sake of clarity the curves referring to $\beta = 2{\cdot}0$ and $\lambda = 8{\cdot}0$ have not been reported in the figure.

In the following figures only the results for $\lambda = 4{\cdot}0$ have been reported because for different slenderness ratios the system response is qualitatively the same and is amplified as the slenderness increases. Figure 4 shows that, for $\varphi_s = 90^\circ$ and $\omega = 10{\cdot}0$, maximum rotation increases according to the friction angle φ_1 up to a peak value and then a plateau is exhibited at about $\varphi_1 = 20^\circ$ for all β values; furthermore, both the peak and the plateau increase according to the excitation amplitude. Figure 5 shows that for $\beta = 4{\cdot}0$ and $\omega = 10{\cdot}0$, maximum rotation increases according to the friction angle φ_1 up to a peak value and then a plateau is exhibited at about $\varphi_1 = 20^\circ$ for all φ_s values. It is worth noting that for $\varphi_s \geqslant 20^\circ$ no significant difference is exhibited by the diagrams. It can be observed that the response for $\varphi_s = \varphi_1 = 15^\circ$ equals that for $\varphi_s = 15^\circ$ and $\varphi_1 = 90^\circ$; similarly the response for $\varphi_s = \varphi_1 = 90^\circ$ and for $\varphi_s = 90^\circ$ and $\varphi_1 = 15^\circ$ are the same. This is the reason why the corresponding curves have not been reported in Figure 3.

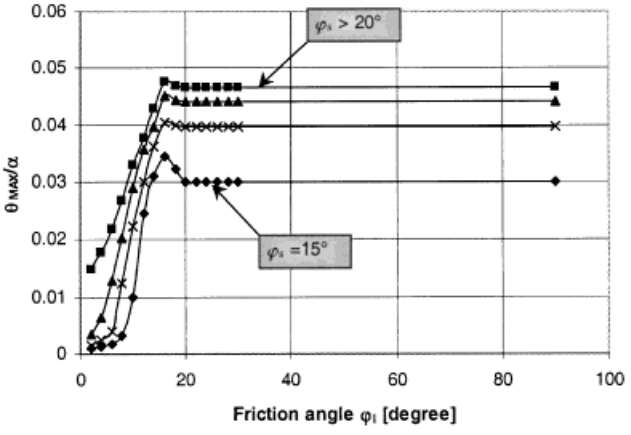

Figure 5. Maximum rotation *versus* friction angle φ_1 for $\beta = 4{\cdot}0$ and $\omega = 10{\cdot}0$

3.2. *Harmonic excitation*

In this case the driving function given by equation (1) holds all along the analysis, as it has been assumed by Sinopoli and Sepe[23] for the trilith and by Spanos and Koh,[5] Tso and Wong,[8,9] Hogan,[10] Andreaus,[11] Shenton and Jones,[12,13] etc. for the single block. As already pointed out in the literature[23] the periodicity and then the stationarity character of such an excitation makes it very different from an earthquake; nevertheless, it can be considered as a necessary preliminary step toward the knowledge of the forced dynamics of the system. Moreover, it should be noted that the persistence of a harmonic excitation for long durations is not realistic, and hence the survivability of such assemblies when subjected to excitations of long duration could be understood by the observation that motion never exceeds a point of recovery.

In agreement with the observations already made in the scientific literature[23] only two cases have been identified: rest and failure. In all the cases where motion has been observed to occur, collapse required only a sufficiently long time enough t^*, unlike the case of half-sine-wave pulse where, even if motion initiates, the collapse does not necessarily occur.

Two different failure modes have been identified: loss of the geometrical configuration for either overall excessive rotation (Figure 1(c), first mode) or coupled effects between excessive slidings and rotation (Figure 1(d), second mode). When the time duration is long enough, the motion exhibits orbitally unstable cycles. Rigorously a steady-state mode is called the (m, n) mode if there are $2m$ impacts in an orbit which repeats itself every n periods of the driving force. In the following the term 'cycle' (m, n) will be used in an approximate way to understand a periodic behaviour limited to a finite time range.

Also in this case of harmonic excitation, in the following figures only the results for $\lambda = 4{\cdot}0$ have been reported because for different slenderness ratios the system response is qualitatively the same: during the transient the maximum rotation is amplified, and the duration time reduces as the slenderness increases.

Figures 6–9 show survival domains for different levels of friction. In this respect, it could be interesting to investigate the nature of the structure of the boundary separating stable (no relative motion) and unstable motions (overturning), as done by Plaut *et al.*[27,28] in the case of a single

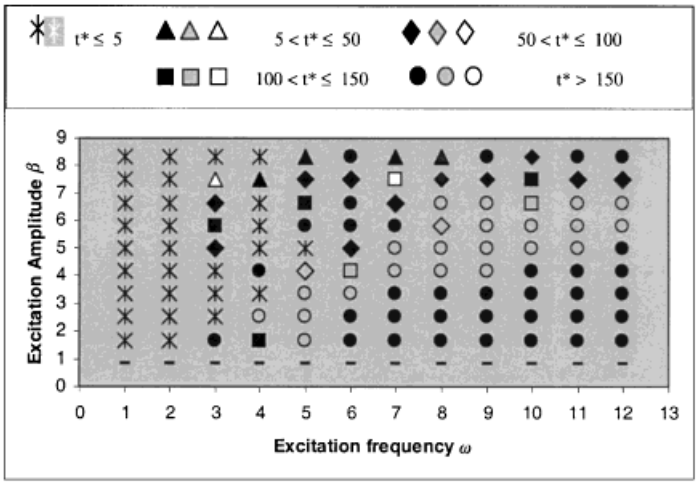

Figure 6. Survival domain ($\varphi_s = \varphi_1 = 90°$)

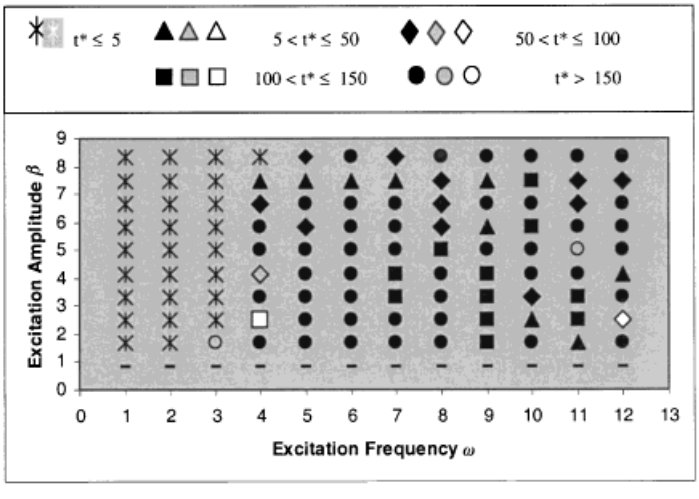

Figure 7. Survival domain ($\varphi_s = \varphi_1 = 15°$)

slender rigid block resting on a rigid and flat foundation and subjected to a see-sawing excitation; sliding and bouncing are not considered and then the system exhibits only one degree-of-freedom;[27,28] the critical boundaries in the plane of excitation amplitude *versus* excitation frequency, separating regions associated with different numbers of impacts, and in particular overturning and non-overturning regions, exhibit certain fractal properties. In order to gain sufficient resolution, the above-mentioned authors adopted a very close mesh in parameter plane feasible for a simple SDOF system. Unfortunately, this kind of refined analysis is cumbersome in the case of the nine degrees-of-freedom system studied in the present paper. Thus, we have limited

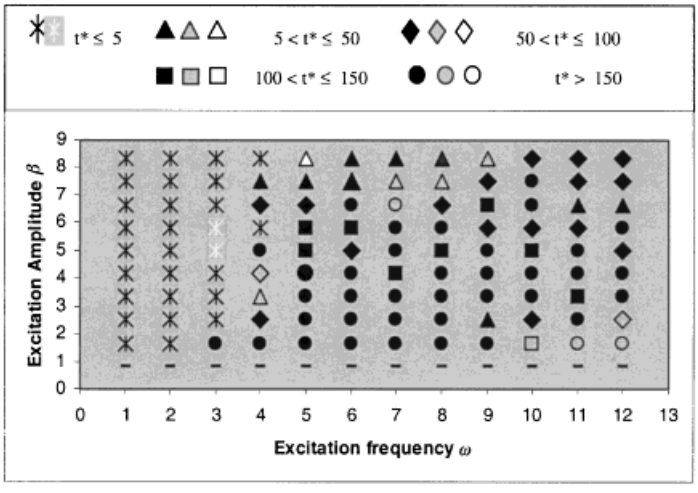

Figure 8. Survival domain ($\varphi_s = 90°$, $\varphi_1 = 15°$)

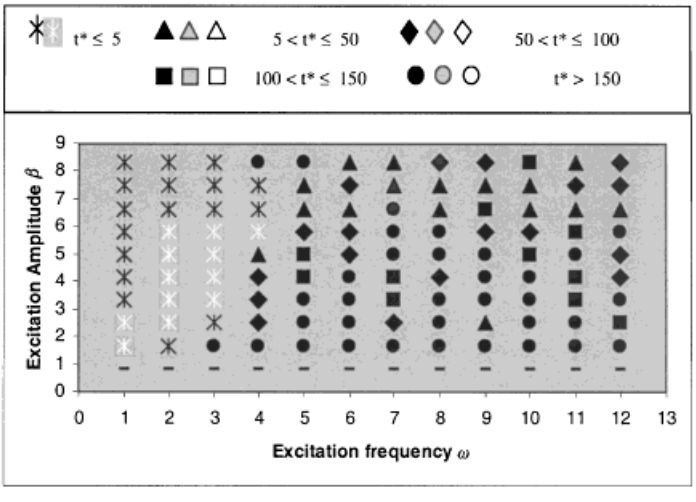

Figure 9. Survival domain ($\varphi_s = 90°$, $\varphi_1 = 5°$)

ourselves to a rough mesh, in Figures 6–9, which, however, is able to give general features of the overturning behaviour. Generally speaking, it can be remarked that increasing excitation frequency and decreasing amplitude do not always increase duration time t^*. As far as the meaning of symbols used in Figures 6–9, black and white stars denote, respectively, first and second modes for very short duration times ($t^* \leqslant 5$ s); triangles, rhombi, squares and circles indicate, respectively, short, medium, long and very long duration times. As far as colours are concerned, black and grey are associated with the second mode; in the former case (black), the cycle that more frequently occurs during the transient is the (1,1) type; in the latter case (grey), cycles

different from the (1,1) type are exhibited, namely (1,3) possibly changing in (2,6), (2,2), and chaotic motion. White colour refers to the first mode, which is exceptionally encountered for $t^* > 5$ s. Figures 6 and 7 show that for $\varphi_s = \varphi_1$ the first mode prevails for $t^* \leqslant 5$ s whereas the second mode predominates for $t^* > 5$ s. Figures 8 and 9 show that, as the difference between φ_s and φ_1 increases, the first mode more often occurs for $t^* \leqslant 5$ s, whereas the second mode is predominant for $t^* > 5$ s.

In the following figures the rotation of the left column has been selected to represent the trilith motion, because the right column attains the same maximum rotation although at a different time. Figure 10 shows the maximum rotation during the transient in terms of excitation frequency, for a given $\beta = 4{\cdot}0$; the cases of equal friction ($\varphi_s = \varphi_1$) at either low (15°) and high (90°) friction have been compared with the case of $\varphi_s \neq \varphi_1$. Figure 11 shows the maximum rotation during the transient in terms of excitation frequency, for given $\varphi_s = \varphi_1 = 90^\circ$ and different values of driving amplitude. Both the diagrams reveal that on the average the maximum transient rotation decreases as the excitation frequency increases. In the particular case of $\varphi_s = \varphi_1 = 90^\circ$, $\beta = 4{\cdot}0$ and $\omega = 10{\cdot}0$, rotation has been sampled at multiples of the driving period (Figure 12); for $0 \leqslant t < 280$ s, the motion exhibits a (1, 3) cycle (Figure 13), and, for $280 < t \leqslant 310$ s, a (2,6) cycle occurs (Figure 14); on the average for $t > 310$ s the collapse takes place. It is worth noting that

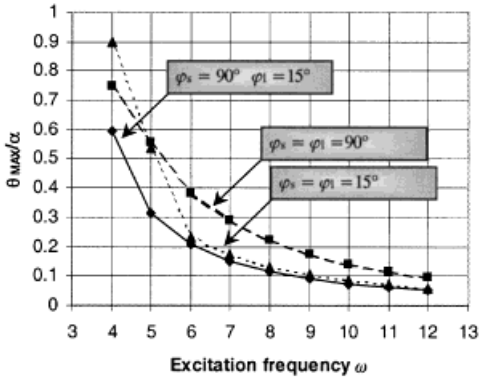

Figure 10. Maximum transient rotation versus excitation frequency for $\beta = 4{\cdot}0$

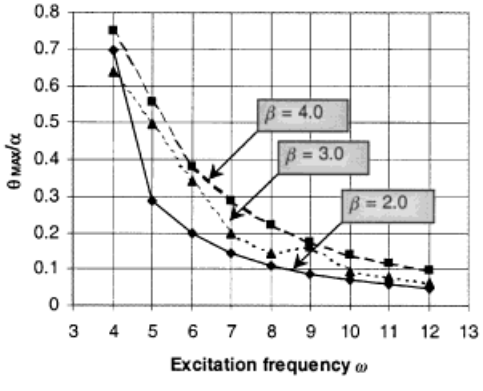

Figure 11. Maximum transient rotation versus excitation frequency for $\varphi_s = \varphi_1 = 90^\circ$

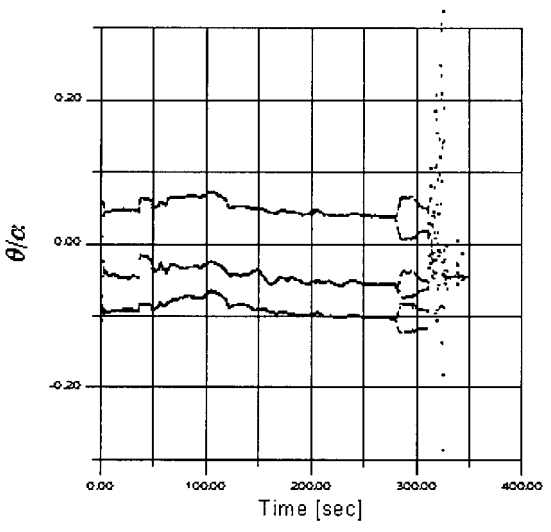

Figure 12. Sampling of the rotation at multiples of the driving period for $\varphi_s = \varphi_1 = 90^\circ$, $\beta = 4{\cdot}0$, $\omega = 10{\cdot}0$

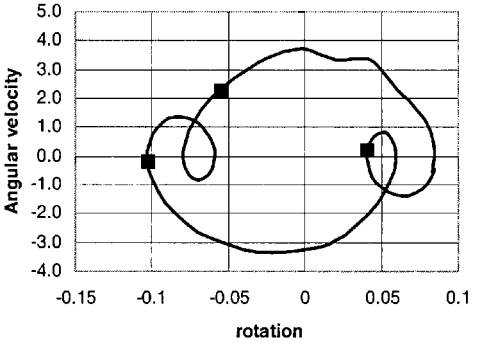

Figure 13. Cycle (1,3) for $\varphi_s = \varphi_1 = 90^\circ$, $\beta = 4{\cdot}0$, $\omega = 10{\cdot}0$, $0 \leqslant t \leqslant 280$ s

a slight bouncing effect is revealed by short branches characterized by constant angular velocity in the neighbourhood of $\theta = 0^\circ$; it was possible to detect such a phenomenon owing to the full degrees-of-freedom system.

Chaotic motion has been detected for $\varphi_s = \varphi_1 = 14{\cdot}7^\circ$ $\omega = 3{\cdot}0$ $\beta = 1{\cdot}664$ (Figure 15). Figure 15(a) shows a typical chaotic trajectory; the impact map is illustrated by Figure 15(b), where the phase is defined as $\Phi = (\Omega t) \bmod (2\pi)$; the ordinate axes reports the angular velocity calculated at time before each impact.

4. CONCLUSIONS

The most interesting features of the dynamic response of the trilith are described below.

As far as the half-sine-wave pulse is concerned, in the survival domains β–ω, three zones have been identified: rest, stable motion and collapse; it has been observed that decreasing friction

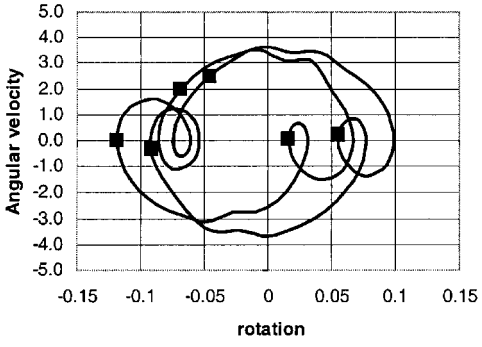

Figure 14. Cycle (2,6) for $\varphi_s = \varphi_1 = 90^\circ$, $\beta = 4{\cdot}0$, $\omega = 10{\cdot}0$, $280 < t \leqslant 310$ s

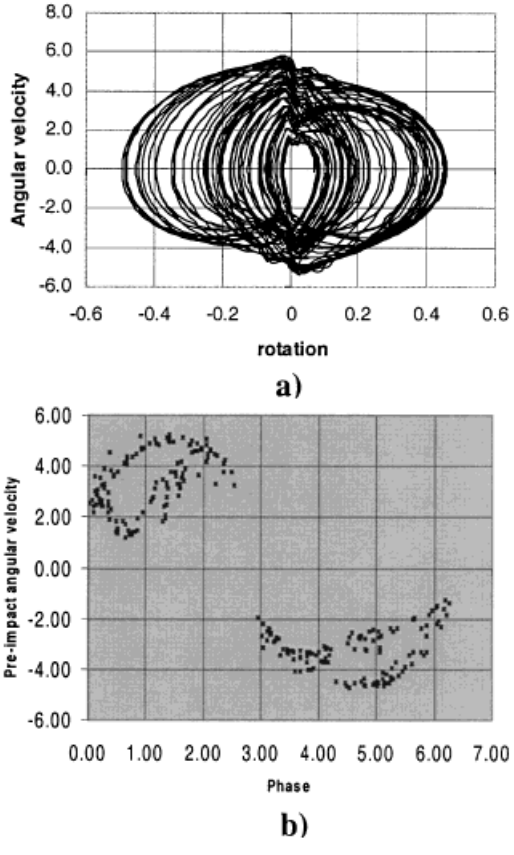

Figure 15. System parameters: $\varphi_s = \varphi_1 = 14{\cdot}70^\circ$, $\beta = 1{\cdot}664$, $\omega = 3{\cdot}0$. (a) Chaotic trajectory; (b) Impact map

widens the stable zone and simultaneously, for given excitation amplitude and frequency, reduces the maximum response. As far as harmonic excitation is concerned, only two cases have been identified: rest and transient up to failure. In all the cases where motion has been observed to

occur, collapse required a sufficiently long time enough, unlike the case of half-sine-wave pulse where, even if motion initiates, the collapse does not necessarily occur. Two different failure modes have been identified: loss of the geometrical configuration for either overall excessive rotation or coupled effects between excessive slidings and rotation. The influence of friction levels on the collapse mode and on the cycle type should be noticed. The investigation has revealed that on the average the maximum transient rotation decreases as the excitation frequency increases. It is worth noticing that, during the transient, a slightly wide variety of responses ranging from (1,1) cycle to chaotic motion has been exhibited. For both the driving excitations, increasing slenderness magnifies the maximum rotation and, for harmonic excitation, reduces the duration time.

ACKNOWLEDGEMENTS

This work was partially funded by the Italian Ministry of University and Scientific Research.

REFERENCES

1. G. W. Housner, 'The behaviour of inverted pendulum structures during earthquakes', *Bull. Seism. Soc. Am.* **53**(2), 403–417 (1963).
2. M. Aslam, W. G. Godden and D. T. Scalise, 'Earthquake rocking response of rigid bodies' *J. Struct. Div. ASCE* **106**, 377–392 (1980).
3. C. S. Yim, A. K. Chopra and J. Penzien, 'Rocking response of rigid blocks to earthquake', *Earthquake Engng. Struct. Dyn.* **8**, 565–587 (1980).
4. Y. Ishiyama, 'Motions of rigid bodies and criteria for overturning by earthquake excitation', *Earthquake Engng. Struct. Dyn.* **10**, 695–650 (1982).
5. P. D. Spanos and A. S. Koh, 'Rocking of rigid blocks due to harmonic shaking', *J. Engng. Mech. ASCE* **10**, 1627–1642 (1984).
6. C. S. Yim and A. K. Chopra, 'Earthquake response of structures with partial uplift on Winkler foundation', *Earthquake Engng. Struct. Dyn.* **12**(2), 203–281 (1984).
7. A. Sinopoli, 'Dynamics and impact in a system with unilateral constraints. The rilevance of dry friction', *Meccanica* **22**(4), 210–215 (1987).
8. W. K. Tso and C. M. Wong, 'Steady state rocking response of rigid blocks. Part 1: Analysis', *Earthquake Engng. Struct. Dyn.* **18**, 89–106 (1989).
9. W. K. Tso and C. M. Wong, 'Steady state rocking response of rigid blocks. Part 2: Experiment', *Earthquake Engng. Struct. Dyn.* **18**, 107–120 (1989).
10. S. J. Hogan, 'The many steady state responses of a rigid block under harmonic forcing', *Earthquake Engng. Struct. Dyn.* **19**, 1057–1071 (1990).
11. U. Andreaus, 'Sliding-uplifting response of rigid blocks to base excitation', *Earthquake Engng. Struct. Dyn.* **19**, 1181–1196 (1990).
12. H. W. Shenton and N. P. Jones, 'Base excitation of rigid bodies. I: Formulation', *J. Engng. Mech. ASCE* **117**, 2286–2306 (1991).
13. H. W. Shenton and N. P. Jones, 'Base excitation of rigid bodies. II: Periodic slide-rock response', *J. Engng. Mech. ASCE* **117**, 2307–2328 (1991).
14. G. Augusti and A. Sinopoli, 'Modelling the dynamics of large block structures', *Meccanica* **27**(3), 195–211 (1992).
15. A. Scalia and M. A. Sumbatyan, 'Slide rotation of rigid bodies subjected to a horizontal ground motion', *Earthquake Engng. Struct. Dyn.* **25**, 1139–1149 (1996).
16. U. Andreaus and P. Casini, 'On the rocking-uplifting motion of a rigid block in free and forced motion: influence of sliding and bouncing' *Acta Mech*, 1–23 (1999).
17. U. Andreaus and P. Casini: 'Rocking-sliding of a rigid block: friction influence on free motion', *Engng. Trans.* **46**(2), 143–164 (1998).
18. K. Muto, H. Takase, K. Horikoshi and H. Ueno, '3-D non linear dynamic analysis of stacked blocks', *Proc. 2nd Special Conf. on Dynamic response of structures: experimentation, observation, prediction and control, Mech. Div., ASCE*, Atlanta, GA, 917–930 (1981).
19. R. Giannini, 'Considerazioni sulla modellazione numerica di sistemi di blocchi rigidi sovrapposti' *Proc. Conf. on Stato dell'arte in Italia sulla meccanica delle murature*, Rome 677–685 (1985) (in Italian).
20. R. H. Allen, I. J. Oppenheim, A. R. Parker and J. Bielak, 'On the dynamic response of rigid body assemblies', *Earthquake Engng. Struct. Dyn.* **14**, 861–876 (1986).

21. C. Blasi and P. Spinelli, 'Un metodo di calcolo dinamico per sistemi formati da blocchi sovrapposti' *Ingegneria Antisismica* **1**(1), 12–21 (1986) (in Italian).
22. I. N. Psycharis, 'Dynamic behaviour of rocking two-block assemblies', *Earthquake Engng. Struct. Dyn.* **19**, 555–575 (1990).
23. A. Sinopoli and V. Sepe, 'Coupled motion in the dynamic analysis of a three block structure', *Appl. Mech. Rev.* **46**(11), part 2, 186–197 (1993).
24. T. Winkler, K. Meguro and F. Yamakazi, 'Response of rigid body assemblies to dynamic excitation', *Earthquake Engng. Struct. Dyn.* **24**(10), 1389–1408 (1995).
25. U. Andreaus and N. Nisticò, 'An analytical-numerical model for contact-impact problems. Theory and implementation in a 2-Dimensional distinct element algorithm', *Comput. Model. Simulation Engng.* **3**(2), 98–110 (1998).
26. C. F. Gerald and P. O. Wheatley, *Applied Numerical Analysis*, Addison-Wesley, Reading, MA, 1994.
27. L. N. Virgin, W. T. Fielder and R. H. Plaut, 'Transient motion and overturning of a rocking block on a seesawing foundation', *J. Sound Vib.* **191**(1), 177–187 (1996).
28. R. H. Plaut, W. T. Fielder and L. N. Virgin, 'Fractal behaviour of an asymmetric rigid block overturning due to harmonic motion of a tilted foundation', *Chaos, Solitons Fractals* **7**(2), 177–196 (1996).

